In situ measurement of electromigration-induced transient stress in Pb-free Sn-Cu solder joints by synchrotron radiation based X-ray polychromatic microdiffraction

Kai Chen[1,2], N. Tamura[1], M. Kunz[1], K. N. Tu[2], and Yi-Shao Lai[3]

1. Advanced Light Source, Lawrence Berkeley National Laboratory, Berkeley, CA 94720
2. Department of Materials Science and Engineering, UCLA, Los Angeles, CA 90095
3. Advanced Semiconductor Engineering, Kaoshiung, Taiwan 811, Republic of China

Abstract

Electromigration-induced hydrostatic elastic stress in Pb-free SnCu solder joints was studied by *in situ* synchrotron X-ray white beam microdiffraction. The elastic stresses in two different grains with similar crystallographic orientation, one located at the anode end and the other at the cathode end, were analyzed based on the elastic anisotropy of the β-Sn crystal structure. The stress in the grain at the cathode end remained constant except for temperature fluctuations, while the compressive stress in the grain at the anode end was built-up as a function of time during electromigration until a steady state was reached. The measured compressive stress gradient between the cathode and the anode is much larger than what is needed to initiate Sn whisker growth. The effective charge number of β-Sn derived from the electromigration data is in good agreement with the calculated value.

I. Introduction

Electromigration (EM) is known to introduce back stress in confined short stripes of Al interconnects [1, 2]. When the atoms move from the cathode to the anode in the stripe under high electric current density, tensile and compressive stresses will be established at the cathode and the anode, respectively. The back stress will eventually counterbalance the electromigration effect, leading to a steady atomic flux state. Building up the back stress gradient takes time, and the length of this time is a function of a number of parameters including electric current density, temperature and atomic diffusivity. The period of stress build-up before it reaches a steady state is called the transient period. Both theoretical analysis and experimental study of the transient state and back stress in Al stripes have been reported [3-5]. However, it is unclear if the transient state also occurs in Cu damascene interconnects and in flip chip solder joints because of differences in the EM-induced atomic diffusion mechanisms. Nevertheless, electromigration-induced Sn whisker growth at the anode in Pb-free solder joints due to current crowding has been reported [6]. Yet, there are few reports in the literature on modeling and measurement of the back stress in flip chip solder joints, because of the complicated line-to-bump configuration in flip chips. At the current crowding region, where the electrons enter into or exit from the solder joint, the electric current density can be one order of magnitude higher than the average current density [7]. Furthermore, since β-Sn has a body-centered tetragonal crystal structure (a = 5.84Å, c = 3.19Å), most of the physical properties are highly anisotropic, including the coefficient of thermal expansion (CTE), diffusivity, Young's modulus, and electrical resistivity. The CTE along the c-direction is about twice of that along the a-direction [8, 9]. At 150 ^{o}C, Cu

diffuses in Sn about 40 times faster along the c-direction than along the a-direction, but the Sn self-diffusivity along the a-direction is about twice of that along the c-direction [10-12]. The stiffness along the c-direction is about 1.2 times of that along the a-direction. The combined effects of current crowding in the solder geometry and the anisotropic structure of Sn result in the complex strain / stress distribution in Sn-based Pb-free solder joints.

High brilliance polychromatic X-ray beam produced by synchrotron radiation source can be focused by a pair of Kirkpatrick-Baez mirrors to submicron size. This was proven to be a powerful tool for microstructure study of polycrystalline materials, as it provides measurement of crystal orientation, strain / stress, dislocation densities [13 - 15]. The data as an array of Laue diffraction patterns are recorded by a 2-dimensional X-ray CCD detector as the sample is raster-scanned under the micro-focused X-ray beam. These Laue patterns can be rapidly indexed and analyzed by software such as XMAS (X-ray Microdiffraction Analysis Software). The previous study performed on the microdiffraction beamline at the Advanced Light Source (ALS), Lawrence Berkeley National Laboratory (LBNL), has revealed that the spontaneous Sn whisker growth is the result of stress-migration caused by the formation of the intermetallic compounds [16]. Near the root of the Sn whiskers, the compressive stress gradient was measured to be about 1 MPa / μm. In this study, we report an *in-situ* electromigration-induced stress measurement using synchrotron radiation based scanning polychromatic X-ray microdiffraction. We observed the transient state of stress build-up in Pb-free Sn-Cu flip chip solder joints.

II. Experimental

The configuration of the flip chip samples used in this experiment was very similar to the ones described elsewhere [17], except that the composition of the solder ball was Sn – 0.7 % (wt) Cu. The flip chip sample was cross-sectioned by first grinding with SiC sand papers to the center of the solder joints, and then polished by submicron Al_2O_3 powders to produce a mirror-like smooth surface (rough surface may influence the accuracy of the strain measurement). Then the cross-sectioned sample was annealed at 150 ^{o}C for 2.5 hours. The annealing time was optimized so that the damages caused by polishing could be eliminated but the Sn crystal grains would not grow too large. Two of the cross-sectioned solder joints were then stressed by electrical current at a temperature of 75 ^{o}C. The average current density was kept constant at 1.25×10^4 A/cm^2 for 100 hours. During this testing period, no electric resistance change was detected. The temperature and the applied current density were medium, comparing to the accelerated EM experiments reported in the literature. There were two reasons for using the medium condition. First, after an EM test at relatively high temperature, say 150 ^{o}C, the surface of the cross-sectioned solder joint could become fairly rough because of atomic diffusion towards the free surface and stress relaxation. Second, more Joule heating would be produced with a higher current density, especially in the current crowding region, and a temperature gradient could exist from the top to the bottom of the solder joint [18, 19], which will lead to variations of lattice parameters due to thermal expansion.

For the EM-induced stress study, before and during the *in-situ* study, the polished solder joint was scanned continuously under the micro-focused X-ray white beam on beamline 12.3.2, ALS / LBNL. The energy range of the white X-ray beam was about 5

keV - 24 keV. The experimental setup was very similar to the one used for *in-situ* EM study on thin film samples [20-23]. The flip chip sample was attached to a copper block containing a cartridge heater perpendicularly to the sample stage and the cross-section of the solder joint was kept at 45° with respect to the incident beam, as shown in Figure 1. The temperature of the heater could be controlled within about $\pm$ 2 ^oC. The X-ray beam was focused by Kirkpatrick-Baez mirrors and the beam size was about 1 μm × 1 μm at the sample surface. A MAR X-ray CCD detector with 133 mm active area diameter was mounted at about 8 cm above the sample and 90° with respect to the incidence beam to record the Laue diffraction patterns. The cross-section of the Sn solder joint was scanned at 3 μm step size. Each scan contained 3000 frames. The Laue patterns were analyzed using the in-house software XMAS. . More details on the Laue X-ray microdiffraction set-up are given in Ref. 14.

III. Results and discussions

By indexing the Laue patterns taken at each step on the Sn solder joint cross-section and combining all the 3000 frames of each scan, orientation maps, grain and grain boundary images can be obtained for each scan. One such map is shown in Figure 2, and it was found that there was no detectable grain growth under the experimental condition after 100 hr of EM test. In Figure 2, the electrons entered the solder bump from the bottom, and exited the bump at the upper left corner. The upper left corner was the current crowding corner, where the current density was about one order of magnitude higher than the average value within the solder bump. The diffraction peak didn't broaden significantly after the EM test, indicating that no, or very little plastic

deformation was induced in this testing period by the applied current density. Some assumptions were made in order to detect and analyze the elastic stress evolution. Most importantly, as for the bulk of the Sn solder joint, it is assumed that the EM test established hydrostatic stresses, unlike the cases of the thin film stripes, such as Al interconnect lines [5, 23, 26]. Related experimental [24] and theoretical studies [3, 25] indeed support hydrostatic stress build-up in tin, even though a stress-free vacancy may cause anisotropic lattice strain in tetragonal b-Sn structure. In the Al interconnect line cases, bi-axial stresses were built up by the EM and shear stress played an important role for the plastic deformation and dislocation flow. However, for the case of Sn solder joint, since the solder ball is a bulk sample, and Sn oxide is a protective oxide in air, it is reasonable to assume that the stress within the solder bump is hydrostatic until the oxide layer is broken when a hillock or whisker is formed and the bump surface becomes rough. For our experimental condition, the sample surface remained smooth after the EM test, indicating that there was no surface relief effect. This assumption is important and necessary for our analysis because white beam Laue diffraction is merely sensitive to the change of shape of the unit cell, e.g., the ratio among the lattice parameters of a, b, and c and angles, but blind to the volume change of the unit cell. In other words, we could not determine the absolute lattice parameters of the Sn crystals before and after EM, if the lattice parameter change is hydrostatic, thus the absolute stress could not be directly calculated. However, with body-centered tetragonal crystal structure, the elastic compliances of β-Sn is anisotropic; the lattice parameter ratio (a/c) would deviate from the stress-free β-Sn value of 5.84Å / 3.19Å , when hydrostatic stress σ is built up in the

solder joint due to EM. To calculate the hydrostatic stress, we have the equation below linking the stress σ to the ratio of the lattice parameters:

$$\frac{c'}{a'} = \frac{c(1+\varepsilon_{cc})}{a(1+\varepsilon_{aa})} = \frac{c(1+\sigma(s_{ca}+s_{cb}+s_{cc}))}{a(1+\sigma(s_{aa}+s_{ab}+s_{ac}))} \tag{1}$$

where c' and a' are the lattice parameters under hydrostatic stress σ; c and a are the stress-free lattice parameters; and s_{ij} is the elastic compliance in the ij direction. As a result of symmetry consideration, $s_{ac} = s_{ca} = s_{cb}$, where the subscript a, b, and c refer to the unit cell axes. The stress σ can be expressed as

$$\sigma = \frac{R-1}{(2s_{ac}+s_{cc})-(s_{aa}+s_{ab}+s_{ac})R} \tag{2}$$

where $R = \frac{1+\varepsilon_{cc}}{1+\varepsilon_{aa}}$, which is obtained by indexing the Laue patterns with XMAS. Hence, using Eq. (2), we can measure the stress in the Pb-free solder joints. In the joint, besides a small amount of Cu-Sn intermetallic compounds, the matrix consists of pure β-Sn.

We have calculated the average stress in two grains in the flip chip sample, one at the anode end marked as Grain I and the other at the cathode end marked as Grain II, in Figure 2. We have studied the stress distribution within each individual grain as a function of EM testing time. One of the reasons why these two grains were chosen was that they had very similar orientations, so that a comparison can be made without the effect of the orientation [12]. There were no obvious trend of tensile stress building up in Grain II, as shown by the red dots in Figure 3, which might be the result of the fact that in general hydrostatic tension is hard to keep in experimental samples; however, compressive stress was built up in Grain I at the anode region and the steady state was achieved when the compression was about 540 MPa within this grain after about 60 hours

of electric current stressing. The distance between the centers of Grain I and Grain II was measured to be about 90 μm from Figure 2. Assuming that a linear stress gradient was built up by the EM test, the stress gradient between Grain I and Grain II at steady state could be calculated to be $\frac{\partial\sigma}{\partial x} = \frac{540MPa}{90\mu m} = 6MPa/\mu m$.

According to the irreversible processes of EM [27], the atomic flux driven by electron wind force and the back-stress gradient has been expressed by the equation

$$J = -C\frac{D}{kT}\frac{d\sigma\Omega}{dx} + C\frac{D}{kT}Z^{*}e\rho j$$

where J is the atomic flux, C is the atomic concentration, D is the effective diffusivity, k is Boltzmann's constant, T is the absolute temperature, dσ/dx is the stress gradient, Ω is the atomic volume, Z^{*} is the effective charge number, e is the elementary charge, ρ is the resistivity, and j is the current density. At steady state and below a certain critical length, the net flux is zero. In our case, since we observed no surface morphology change, we assume that the net flux is very small. When the steady state is reached, Z^{*} can therefore be calculated:

$$C\frac{D}{kT}\frac{d\sigma\Omega}{dx} = C\frac{D}{kT}Z^{*}e\rho j.$$

and thus:

$$Z^{*} = \frac{\Omega}{e\rho j}\frac{d\sigma}{dx},$$

Z* can be calculated by knowing the stress gradient and ρ and j. Based on a former study [28], the current density at the anode corner where the electrons entered into the solder joint is about an order of magnitude higher than the average current density in the bulk of the solder joint. We obtain the effective charge number Z^{*} to be 24 when we take the

stress gradient = 6 MPa / μm, ρ_{Sn} = 1.325 × 10^{-7} Ω-m, and j = 1.25 × 10^5 A/cm^2, which was 10 times of the average current density than we applied. The value of Z* is close to the reported value of 18 for self-electromigration in bulk Sn [29].

A possible error of the measured effective charge number may come from the stress gradient measurement, including the hydrostatic stress assumption and the influences from the temperature gradient caused by Joule heating. Even though we have stated that the assumption of the purely hydrostatic stress is reasonable in general, it must be noted that we should not neglect the interactions among the neighboring grains. As we have reported, grain rotations induced by EM have been observed in Pb-free solder joints, which is a piece of evidence that shear stress was induced in this procedure [30]. On the other hand, the deviation from this assumption is expected to be minimized by averaging the stress within each whole grain because the interaction among the neighboring grains in the bulk solder joint is almost symmetric.

To estimate the error caused by Joule heating, we assume the real temperature at the current crowding region to be 75 °C + ΔT, so that the error of the compressive stress calculation from ignoring the temperature difference due to Joule heating is

$$\sigma = \frac{\tau - 1}{(2s_{ac} + s_{cc}) - (s_{aa} + s_{ab} + s_{ac})\tau}$$

where $\tau = \frac{1 + E_c \Delta T}{1 + E_a \Delta T}$, s_{ij} has the same physical meaning as described before, and E_a and E_c are the CTE of β-Sn in a-direction and c-direction, which were reported to be 15.4 × 10^{-6} and 30.5 × 10^{-6} / °C, respectively [10]. According to a previous study, the temperature difference ΔT caused by electric current would be no more than 5 °C for the current density we applied in this experiment [18], so that the measuring error caused by

the Joule heating is about -120 MPa, where the minus sign indicates compressive stress. This number is about 4 times smaller than the measured steady state compression, meaning our measurement of stress build-up is reliable. If we take the temperature gradient into account, the stress gradient at the steady state can be calibrated as $\frac{\partial \sigma}{\partial x} = \frac{(540-120)MPa}{90\mu m} = 4.7MPa/\mu m$ and the effective charge factor Z^* becomes 19.

The above estimation of the error of the stress measurement caused by Joule heating is also applicable for understanding the fluctuation of the measured average stress within Grain II. From Figure 3, the fluctuation of the stress in Grain II during the measurement period was about ± 100 MPa, indicating that the correspondingly temperature fluctuation was within ± 5 ^{o}C, which is reasonable considering the capability of the copper cartridge heater. More detailed discussion of the effect of temperature on EM and back stress gradient will be reported in a forthcoming paper.

Additional energy scan using monochromatic X-ray beam need be performed at each spot of the solder ball cross-section, so that the absolute strain / stress tensor can be directly obtained without the assumption of hydrostatic stress, and the strain / stress distribution can be precisely profiled. However, monochromatic X-ray diffraction requires longer exposure time and increased amount of beamtime which was not available at the time of the present study.

IV. Conclusion

In summary, we studied the distribution and evolution of the EM-induced compressive stress at the anode where current crowding occurs in Sn-based Pb-free flip chip solder joints by synchrotron X-ray white beam Laue microdiffraction. The effective

charge number for SnCu solder is calculated and found to be in reasonable agreement with the value reported in a previous study. The compression stress gradient within the solder ball was also estimated, and the possible errors were discussed. The compressive stress gradient is higher than the stress gradient reported for the spontaneous Sn whisker growth, supporting the finding that Sn whiskers can be squeezed out at the current crowding region at the anode end in the Pb-free flip chip solder joints induced by EM.

Acknowledgment: The authors at UCLA would like to acknowledge the support from SRC contract KJ-1772 and Seoul Technopark. The Advanced Light Source is supported by the Director, Office of Science, Office of Basic Energy Sciences, Materials Science Division, of the US Department of Energy under Contract No. DE-AC02-05CH11231 at Lawrence Berkeley National Laboratory. The micro-diffraction program at the ALS on beamline 12.3.2 was made possible by NSF grant # 0416243. One of the authors (K. C.) thanks Dr. J. O. Suh at JPL for helpful discussions.

References

1. I. A. Blech, J. Appl. Phys. **47** (4), 1203 (1976)
2. I. A. Blech and C. Herring, Appl. Phys. Lett. **29** (3), 131 (1976)
3. M. A. Korhonen, P. Børgessen, K. N. Tu, and C. -Y. Li, J. Appl. Phys. **73**, 3790 (1993)
4. J. J. Clement, and C. V. Thompson, J. Appl. Phys. **78**, 900 (1995)

5. P. C. Wang, G. S. Cargill III, I. C. Noyan, and C.-K. Hu, Appl. Phys. Lett. **72**, 1296 (1998)

6. F. -Y. Ouyang, K. Chen, K. N. Tu, and Y. -S. Lai, Appl. Phys. Lett. **91**, 231919 (2007)

7. E. C. C. Yeh, and K. N. Tu, J. Appl. Phys. **88**, 5680 (2000)

8. W. P. Mason, and H. E. Bommel, J. Acoust. Soc. Amer. **28**, 930 (1956)

9. H. B. Huntington, in *Diffusion in Solids: Recent Development*, edited by A. S. Nowick and J. J. Burton (Academic, New York, 1974), p. 303.

10. B. F. Dyson, T. R. Anthony, and D. Turnbull, J. Appl. Phys. **37**, 3408 (1967)

11. F. H. Huang, and H. B. Huntington, Phys. Rev. B **9**, 1479 (1974)

12. M. H. Lu, D. -Y. Shih, P. Lauro, C. Goldsmith, and D. W. Henderson, Appl. Phys. Lett. **92**, 211909 (2008)

13. I. C. Noyan, and J. B. Cohen, *Residual Stress – Measurement by Diffraction and Interpretation*, Springer, Heidelberg (1987)

14. M. Kunz, N. Tamura, K. Chen, A. A. MacDowell, R. S. Celestre, M. M. Church, S. Fakra, E. E. Domning, J. M. Glossinger, D. W. Plate, B. V. Smith, T. Warwick and H. A. Padmore, Review of Scientific Instruments, accepted

15. N. Tamura, A. A. MacDowell, R. S. Celestre, H. A. Padmore, B. Valek, J. C. Bravman, R. Spolenak and W. L. Brown, Appl. Phys. Lett. **80**, 3724 (2002)

16. W. J. Choi, T. Y. Lee, K. N. Tu, N. Tamura, R. S. Celestre, A. A. MacDowell, Y. Y. Bong, and L. Nguyen, Acta Mater. **51**, 6253 (2003)

17. A. T. Huang, A. M. Gusak, K. N. Tu, and Y. -S. Lai, Appl. Phys. Lett. **88**, 141911 (2006)

18. H. -Y. Hsiao, and C. Chen, Appl. Phys. Lett. **90**, 152105 (2007)

19. D. Yang, B. Y. Wu, Y. C. Chan, and K. N. Tu, J. Appl. Phys. **102**, 043502 (2007)

20. B. C. Valek, J. C. Bravman, N. Tamura, A. A. MacDowell, R. S. Celestre, H. A. Padmore, R. Spolenak, and W. L. Brown, Appl. Phys. Lett. **81**, 4168 (2002)

21. A. T. Wu, K. N. Tu, J. R. Lloyd, N. Tamura, and B. C. Valek, Appl. Phys. Lett. **85**, 2490 (2004)

22. A. S. Budiman, W. D. Nix, N. Tamura, B. C. Valek, K. Gadre, and J. Maiz, Appl. Phys. Lett. **88**, 233515 (2006)

23. K. Chen, N. Tamura, B. C. Valek, and K. N. Tu, J. Appl. Phys. **104**, 013513 (2008)

24. L. Xu, J.H.L. Pang, and K.N. Tu, Appl. Phys. Lett. **89**, 221909 (2006)

25. Y. Liu, L. Liang, S. Irving, and T. Luk, Microelectron. Reliab. **48**, 811 (2008)

26. H. Zhang, G. S. Cargill, III, Y. Ge, A. M. Maniatty, and W. Liu, J. Appl. Phys. **104**, 123533 (2008)

27. K. N. Tu, J. Appl. Phys. **94**, 5451 (2003)

28. L. Y. Zhang, S. Q. Ou, J. Huang, K. N. Tu, S. Gee, and L. Nguyen, Appl. Phys. Lett. **88**, 012106 (2006)

29. K. N. Subramanian, Fatigue Fract. Eng. Mater. Struct. **30**, 420 (2007)

30. K. Chen, N. Tamura, and K. N. Tu, Mater. Res. Soc. Symp. Proc. **1116E**, I05-06, 2009

Figure captions

Figure 1 Scheme of sample and detector positions

Figure 2 Orientation map of the solder bump and the direction of the electric current

Figure 3 Stress evolutions in individual grains at the anode and cathode end, respectively

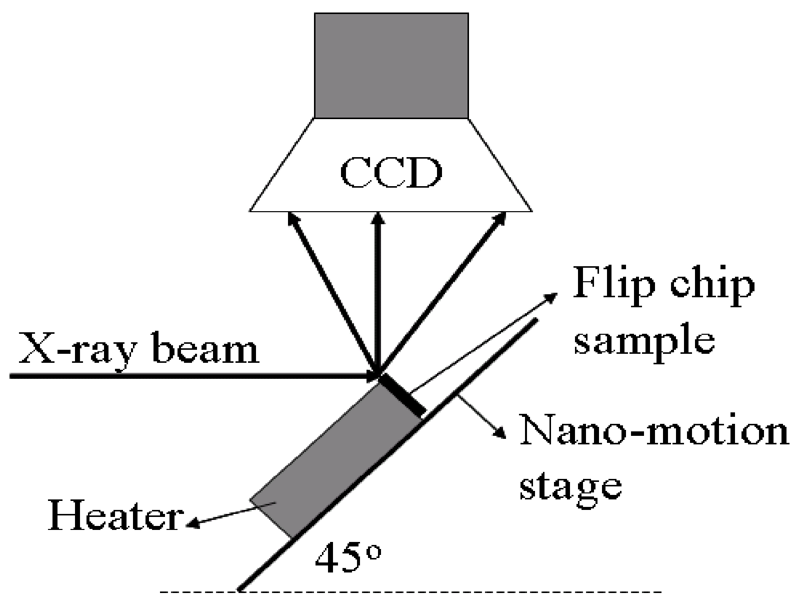

Figure 1 Scheme of sample and detector positions

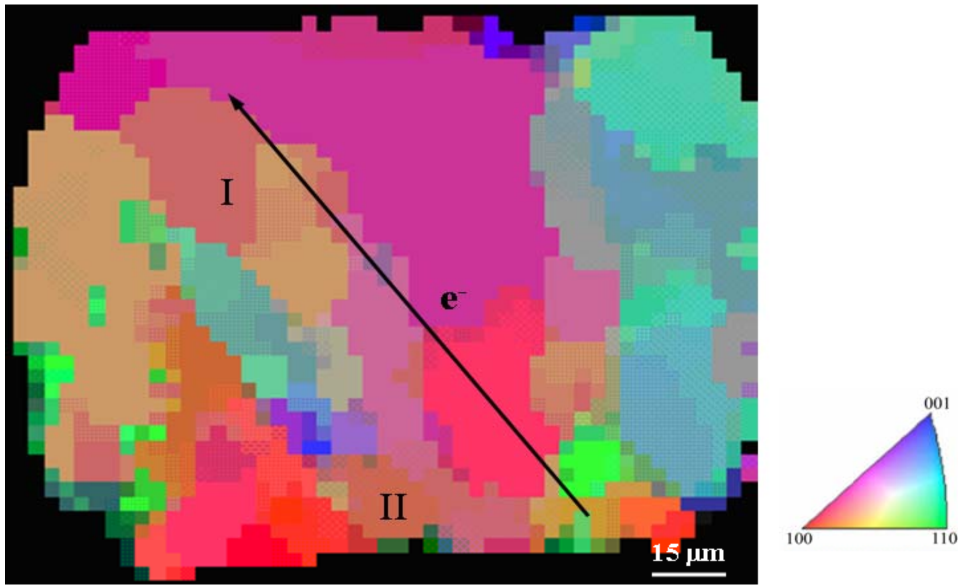

Figure 2 Orientation map of the solder bump and the direction of the electric current

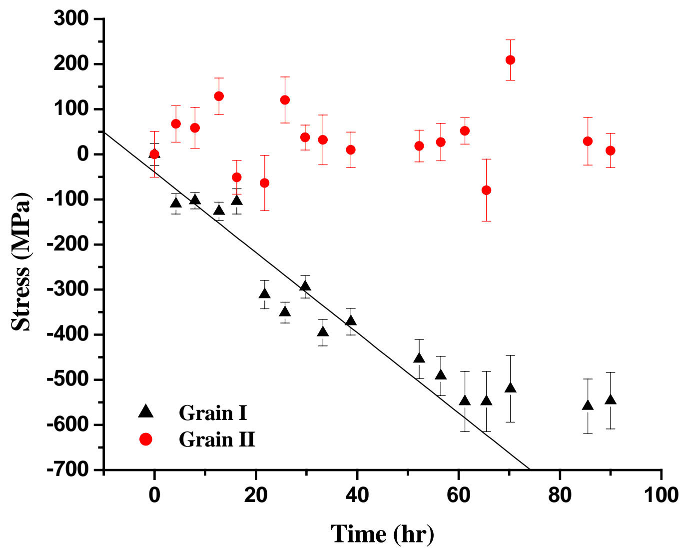

Figure 3 Stress evolutions in individual grains at the anode and cathode end, respectively